 Bull. Chem. Soc. Jpn., 75, 2555–2569 (2002)

Accounts

Ab Initio Direct Molecular Dynamics Simulations and QM/MM Computations in Search of Organic Reaction Mechanisms

Hiroshi Yamataka* **and Misako Aida*,†**

Institute of Scientific and Industrial Research, Osaka University, Ibaraki, Osaka 567-0047

†Department of Chemistry, Graduate School of Science, Hiroshima University, Kagamiyama, Higashi-Hiroshima 739-8526

(Received April 11, 2002)

Ab initio direct-MD simulations and combined QM/MM computations are the theoretical methods that are expected to play an important role in the study of organic reaction mechanisms in the near future. This account reviews recent achievements with these methods in mechanistic studies of organic reactions. In particular the focus is placed on proton transfer, S_N1, S_N2, and S_N2/ET borderline reactions as illustrative examples. The direct-MD simulations revealed the importance of dynamics in controlling the reaction path, which can often be different from the minimum energy path on the potential energy surface. It was also demonstrated that the QM/MM computations could be a promising method to analyze reactions in solution.

The role of computational chemistry in studying mechanisms of organic reactions has become increasingly important in recent years due to rapid advances in computer technology and software development. In particular, calculations of the structures and energies of initial state, transition state (TS), and product state as well as calculations of minimum energy path on the potential energy surface give invaluable insights into the reaction mechanism that cannot be obtained from experiments. Ab initio calculations are now able to provide us information about chemical reactions of acceptable accuracy, although the system to be calculated is practically limited to medium size species in the gas phase. For deeper mechanistic study of organic reactions, further advances of the computational method are required in two directions: one toward the analysis of the effects of temperature and dynamics on reaction mechanism and the other toward the computation of large systems, such as supramolecules, proteins, and solutions. Molecular dynamics (MD) simulations and combined quantum mechanical/molecular mechanics (QM/MM) computations are promising methods for these purposes.

Molecular dynamics simulations are widely used in many fields of chemistry, ranging from inorganic materials to biological systems. The classical MD method[1] is based on an analytical potential energy surface, which is generally constructed by a fit to potential energies obtained from ab initio molecular orbital (MO) calculations for a large number of geometrical configurations. It is very laborious and impractical, if not impossible, to construct empirical potential functions to describe systems with many atoms. In addition, it is, in principle, not easy to ensure the reliability of the potential functions thus obtained for reaction systems which involve forming and breaking bonds. One alternative approach is to calculate the classical trajectories directly by utilizing ab initio QM methods without constructing the potential energy surface. The advantage of the direct-MD method is that the reliability of the results is readily evaluated in terms of the level of theory and the basis set used. The disadvantage of this method, on the other hand, is that ab initio trajectory calculations require much more computing time than traditional trajectory calculations on a model potential energy surface and thus it is not feasible to calculate a large number of trajectories for obtaining statistical quantities such as cross sections and energy distributions. It is difficult at present to carry out statistical sampling to obtain reliable kinetic data from direct MD calculations. Nonetheless, individual trajectories for a particular kinetic energy provide examples of those dynamical processes, and provide valuable information on the chemical processes at the molecular level. Therefore, in spite of such limitations, the direct MD method has become increasingly popular, either with semi-empirical[2] or ab initio[3–12] quantum chemical theories. With the rapid advances in computer technology, it is now becoming practical to use ab initio level calculations as the energy and force generators. In many of these direct dynamic studies, the MD approach served as a means to probe phase space in search of low energy structures. A few of the studies were concerned with the characterization of chemical reactions.

A fundamental goal of such dynamics studies of chemical reactions is to obtain a microscopic picture of how energy flows and atoms move during the course of a chemical reaction. Recently it has become possible to obtain the same level of detail from real-time femtochemistry experiments, in which one observes the motion of the atoms involved in the chemical reaction. Molecular dynamics can give a complete picture of the reaction event and the results are, in principle, comparable with the experiments.

Although the direct-MD simulation method has become increasingly popular in recent years, it is expensive to calculate analytical gradients at every time step, and so the purpose of the simulations should be different from the purposes of conventional methods using empirical potentials. Several limitations in the direct MD simulations are: (1) the number (tens rather than thousands) and length (ps rather than ns) of trajectories are limited, which means that statistical averages would be poor. (2) The level of ab initio theory that can be used in MD is not generally quantitatively accurate. (3) The systems studied are typically limited to classical dynamics on the ground-state potential energy surface. Despite these limitations, this technique has so far been used to gain considerable qualitative insight via a representative set of trajectories in rather small systems in the gas phase, such as S_N2,[13–16] proton transfer,[17,18] fragmentation,[7,19–24] molecular isomerization,[25,26] electron transfer,[27,28] and others.[29–32]

Computational study of chemical reactivities in solution requires a method to generate and explore the potential energy surface for very large systems. Calculation of the chemical properties with acceptable accuracy needs the use of quantum-theoretical procedures, which consequently, makes the calculation expensive since large systems imply many electrons. Furthermore, characterization of the energy surface requires exploration of hyperspaces with very high dimensionality for a large system particularly a system in solution. One of the most promising methods to solve these problems is a combined QM/MM procedure, in which quantum-mechanical treatment of chemical bond making and breaking events is combined with molecular mechanics description of the surrounding solvent. There are still few examples that carry out optimizations of minima and saddle points by using the QM/MM procedure,[33–35] but this certainly will be the future method of choice in the study of the reactivity in solution.

The present account illustrates how these methods can be applied to organic reactions and discuss what we can expect from further advancement of these methods in the near future. We concentrate on proton-transfer, S_N2, S_N1, and ET/S_N2 borderline reactions, since they serve as illustrative examples for the usefulness of the computational methods. The results provide fundamental insight into the organic reaction theory. For methods that are not described in this article, such as Monte Carlo simulations and Car-Parrinello approach, readers are advised to refer to other sources.[3,36,37]

Proton Transfer

Hydrogen-bond interactions and proton-transfer reactions often play a crucial role in chemical and biological systems. Since proton-transfer reactions are among the simplest reactions in organic chemistry, it would be beneficial to see what we can obtain from MD simulations of this type of reactions. Hydrated oxonium ions, $H_3O^+(H_2O)_n$, are known to play an important role in proton-transfer reactions in aqueous solution.[38] The prototype of hydrated oxonium ions is dioxonium ion ($H_5O_2^+$), whose properties have been studied extensively [39–42] by MO calculations with several levels of theory. Results indicate that the equilibrium structure highly depends on the basis set and on the level of theory employed.

In the study shown here,[43] ab initio MD simulations were carried out for the proton-transfer reaction of the simplest system, $H_5O_2^+$. First of all, ab initio MO calculations were performed at the Hartree–Fock (HF) level of theory with the 6-31G* basis set, with some additional calculations with the 6-311G** basis set and at the MP2 level of theory. The stationary structures were identified by means of a full analysis of the vibrational frequencies. Ab initio direct-MD simulations were then performed, starting from the local minimum. Energies and forces were obtained using the HF/6-31G* level of theory. A step size of 0.5 fs was used for the simulations. The temperature of the system is associated with the classical kinetic energy, and the constant temperature algorithm of Berendsen et al.[44] was used. The program package of HONDO[51] was used for these calculations.

Molecular orbital calculations revealed that the C_2 structure corresponds to the energy minimum at a higher level of theory, while the structure corresponds to the TS at a lower level of theory with a rather small basis set. At the HF/6-31G* level of theory, the central barrier height is small and the energy of the symmetrical structure is even lower than the minima in both sides if the zero-point energies (ZPE) are added. A series of calculations with fixed distances between the two oxygen atoms ($R_{O–O}$) revealed that the central barrier height strongly depends on $R_{O–O}$. Thus, the barrier height of the proton transfer is very high at larger values of $R_{O–O}$ (> 2.5 Å), whereas it reduces remarkably with smaller values of $R_{O–O}$ ($\sim$2.4 Å) and vanishes at very small $R_{O–O}$ (< 2.3 Å). The energy profile at HF/6-311G** was similar to that of HF/6-31G*. At MP2/6-31G* and MP2/6-311G**, the midpoint of the energy profile becomes a minimum in fully relaxed calculations; i.e., the potential is a curve with a single well. It is noted that the optimum $R_{O–O}$ is shorter with a higher level of theory, and that at shorter $R_{O–O}$ the potential is that of a single well even at the HF level of theory. It is probable that the difference in the characteristics of the potential, i.e., single-well or double-well, simply depends on the O–O distance. At any level of theory, the proton is shared by the two oxygen atoms in $H_3O^+(H_2O)$ at a short O–O distance.

Ab initio direct-MD simulations were carried out for the system of $H_3O^+(H_2O)$ as the simplest example of reactions, in which the reaction (proton transfer) proceeds with a low barrier. All the hydrogen atoms are replaced by deuterium in the simulations so that the tunneling effect is not important. The barrier height of the proton transfer is 0.52 kcal/mol (without taking account of ZPE) at HF/6-31G*. The point of interest here is how close to or how far from the TS structure the reaction proceeds.

Figure 1 shows the variations of atomic distances in one of the direct-MD trajectories. In Fig. 2 are shown the structures of the optimized reactant and TS, together with selected snap-

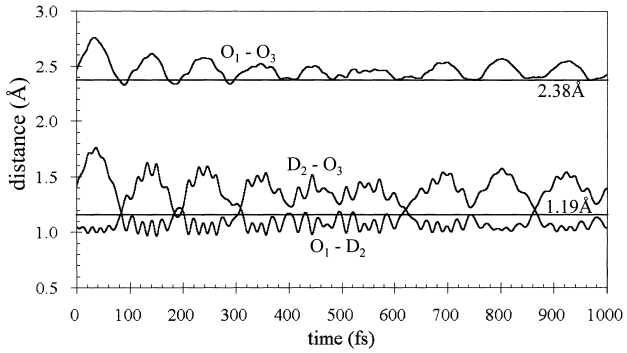

Fig. 1. The atomic distance variations in the ab initio MD simulation (HF/6-31G*) of dioxonium ion at 300 K. All the hydrogen atoms are replaced by deuterium. The lines (2.38 Å and 1.19 Å) indicate the distances in the TS structure.

shot structures along the trajectory. It is seen in Fig. 1 that the shift of the hydrogen and the O–O bond stretch synchronize to each other and that the proton transfer occurs several times during the trajectory when R_{O-O} becomes short. At each point with identical O–D bond distances, the O–D distance somewhat differs from that at the TS determined by MO calculations. Snapshot structures in Fig. 2 clearly show that the O–O distance is also different from that at the TS. Thus, the present simulations indicate that the proton transfer proceeds not through the exact TS structure but through a region close to it. It can be assumed that such a phenomenon would also happen in other type of reactions. Finally, an important implication obtained from the present simulations is that the compression of the O–O bond distance is essential to facilitate the proton transfer between two oxygen atoms. Thus, proton transfer in geometrically rigid systems would be more difficult than that in flexible systems.

S_N2 Reaction

S_N2 reactions of methyl halides with halide anions are one of the reactions most frequently studied with computational methods, since they are, like proton transfer, typical group-transfer reactions whose reaction profiles are simple. Several direct-MD simulations were reported, both with semi-empirical and ab initio theories. In 1996, Hase et al. reported direct dynamics simulations of the reaction, Cl^- + CH_3Cl, using semi-empirical AM1 theory with two different sets of specific reaction parameters (SRP1 and SRP2).[15a] The simulations were started at the $Cl^-\cdots CH_3Br$ complex with different initial non-random energy distributions and the total energy was the harmonic zero-point energy of the complex plus approximately 2.7 kcal/mol. Excitation of different internal modes of the complex leads to different results. The mode-specific dissociation trajectories were compared with previous results using analytical potential functions.[15b] Importantly the study showed that different potential energy surface gave quantitatively different dynamics. The direct dynamics quasiclassical trajectory study of the Cl^- + CH_3Cl S_N2 was later carried out at the ab initio (HF/3-21+G*) level.[14] From the trajectories initiated at the barrier top the product energy partitioning was analyzed. It was shown that extensive CH_3Cl vibrational excitation is needed to access the frontside reaction pathway. Direct ab initio (HF/3-21+G*) dynamics studies were also performed for F^- + CH_3Cl and $F(H_2O)^-$ + CH_3Cl, in which the reaction modes and the energy partitioning into the modes were analyzed.[16]

S_N2 reactions are classified into two types: type I is the reaction of neutral substrate with charged nucleophile and type II is the reaction of neutral substrate with neutral nucleophile.[45] In

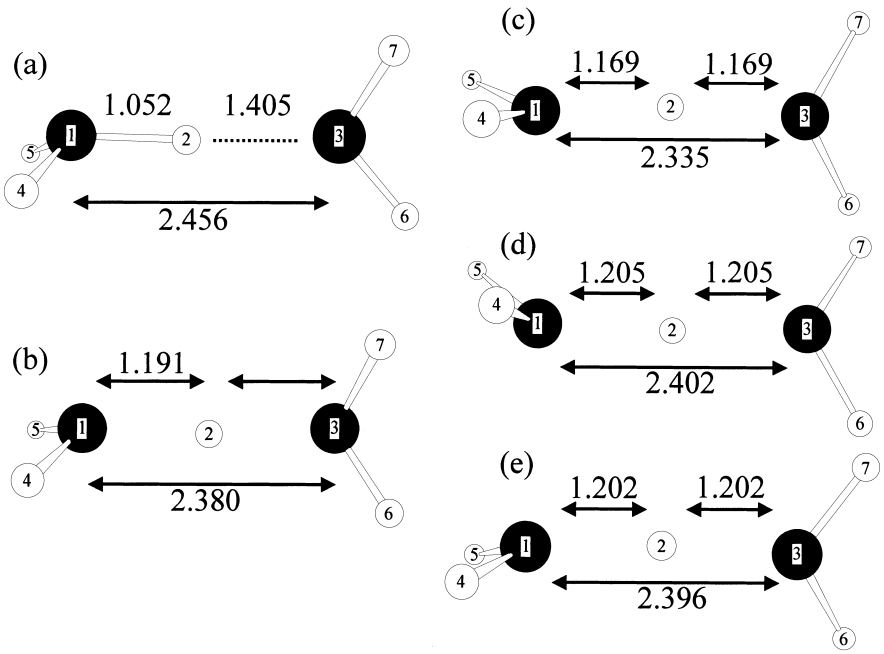

Fig. 2. (a) Optimized structure of $H_3O^+(H_2O)$ at HF/6-31G*. (b) TS structure. (c) A snapshot structure at 184.0 fs of ab initio MD simulation with HF/6-31G*. (d) A snap shot at 621.5 fs. (e) A snap shot at 864.7 fs. Selected atomic distances are shown in Å.

contrast to the cases of type I reactions, the number of computational studies for type II S_N2 is limited because the reaction generates an ion pair in the product state and hence it necessarily experiences a strong solvent effect. Therefore, it is a challenge to perform MO as well as MD studies on this type of reactions.[13,46]

The hydrolysis of methyl chloride (Eq. 1) is a type II S_N2 reaction. The attacking species is a water molecule, which initially loses a proton to a solvent water molecule with the hydroxide ion formally substituting the chloride ion in methyl chloride. Thus during hydrolysis, bond breaking and bond formation involving both solute and solvent molecules take place. It is essential, therefore, to consider the solvent molecules explicitly in modeling the methyl chloride hydrolysis. This is in contrast to type I S_N2 reactions, such as the reaction of a halide anion with methyl halide, in which bond breaking and bond formation occur only in the solute molecules and the solvent molecules do not participate actively in the reaction except as a medium. Direct MD simulations of this type of reactions have previously been carried out as described above and the product energy partitioning and the lifetime of the encounter complex were analyzed.[14–16]

$$n\mathrm{H_2O} + \mathrm{CH_3Cl} \rightarrow \mathrm{HOCH_3} + (n-1)\mathrm{H_2O} + \mathrm{HCl} \quad (1)$$

Ab initio MO investigations of the methyl chloride hydrolysis have shown that the reaction energies and the kinetic parameters of the hydrolysis reaction in aqueous solution are well described in the system of CH_3Cl with 13 water molecules.[46] Moreover, hydrogen-bonded networks of solvent molecules, which exist in the reactant and product complexes and in the TS complex as well, link the attacking water molecule and the leaving chloride atom. A similar network is also present in the smallest cluster with three water molecules, and proton transfers along the hydrolysis reaction path appear both in the 13-water and the 3-water systems. Therefore, the 3-water system can be used as a model system to explore the dynamics of the methyl chloride hydrolysis. The direct-MD simulations for the reaction of methyl chloride with 3 water molecules have been carried out, regarding it as a prototypical model of the larger cluster and of the reaction in solution.[13] The calculation of the intrinsic reaction coordinate (IRC)[47,48] allows a full characterization of the reaction mechanism, but the IRC path is obtained under the constraint that the velocity at any given point along the path is zero. At finite temperature, energy flows among the internal vibrations of the solute as the reaction proceeds, and thus the finite temperature pathway may differ from the IRC path.

Stationary Points along the Reaction. Figure 3 shows the structures and the relative energies of the stationary points of the S_N2 reaction of the methyl chloride hydrolysis obtained at the HF/6-31G level, which include the initial complex (loosely bound state of CH_3Cl and water cluster), the reactant complex (complex-R), the TS, the product complex (complex-P1), the second product complex (complex-P2), and the final product (complex-F). The IRC path shows that TS connects complex-R and complex-P1. Complex-P2 has a direct hydrogen-bond interaction between the H_{1b} atom and the Cl ion. This interaction brings additional stability to the system. In

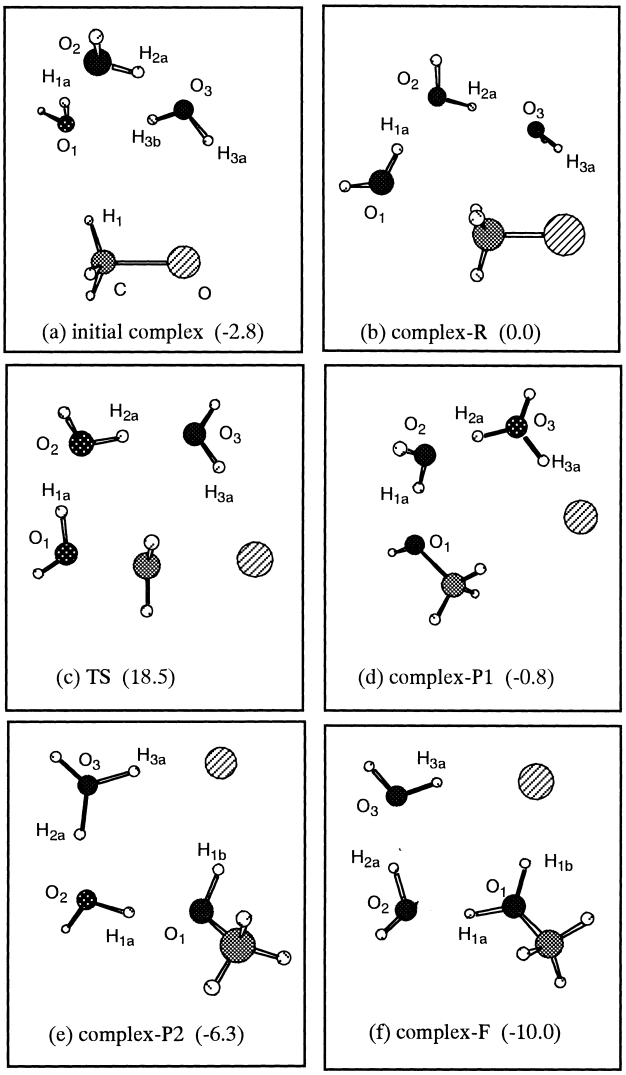

Fig. 3. Structures of the stationary points for MeCl hydrolysis obtained at the HF/6-31G level. Relative energies (in parentheses) are in kcal/mol.

complex-F, H^+ exists in the form of $CH_3OH_2^+$ rather than H_3O^+, consistent with a stronger basicity of CH_3OH than H_2O, and Cl^- is hydrogen-bonded to the proton of $CH_3OH_2^+$, the most acidic proton in the system. The experimental activation enthalpy of the methyl chloride hydrolysis is 26.6 kcal/mol in aqueous solution,[49] and the reaction enthalpy is estimated to be -6.9 kcal/mol from the data of standard heats of formation in aqueous solution.[50] In the 3-water system, if complex-R is taken as the initial state of the reaction, the calculated activation enthalpy is in reasonable accord with the experimental activation enthalpy in spite of the limited number of water molecules included in the system and the small basis set used.

Direct-MD Simulations. Direct-MD simulations were carried out starting at the TS structure with the program package of HONDO.[51] Energies and forces were obtained at HF/6-31G. The classical nuclear trajectories were obtained using a fourth-order gear predictor-corrector algorithm;[1] the temperature of the system is associated with the classical kinetic energy, and the constant temperature (298 K) algorithm of

Berendsen et al.[44] was used. Nine simulations were carried out with different initial velocities starting from the TS. In three of the simulation runs, the system was found to evolve in the backward direction, i.e. to move toward the initial state via the complex-R region, and in the other runs, the trajectories proceeded in the forward direction toward the product state.

Forward Reaction, 1. Figure 4 shows one of the simulations corresponding to the forward run. The O–H distance curves show that the trajectory is made up of three regions: a TS region for the first 100 fs, followed by a proton transfer region for the next 40 fs and then by a product region. In the TS region, the first peak in the atomic charge of the attacking O_l atom around 75 fs (Fig. 4b) corresponds to a three bond build-up on the O_1 atom as a result of the shortening of the C–O_1 bond in Fig. 4c. The system then enters the proton transfer region, in which a proton relay occurs. The first peak in the atomic charge of the O_2 atom around 120 fs (Fig. 4b) corresponds to the formation of H_3O^+ (the first solvent molecule), which coincides with the bond formation of H_{1a}–O_2 as shown in Fig. 4d. The first peak in the atomic charge of the O_3 atom around 130 fs (Fig. 4b) corresponds to the formation of a H_3O^+ molecule (the second solvent water), which coincides with the bond formation of H_{2a}–O_3 as shown in Fig. 4e, indicating a proton transfer to the second solvent water. These structural changes along the trajectory are seen in Fig. 5a–f. After this nearly concerted proton-transfer process, the system reaches the complex-P1 region around 150 fs. Here, the complex-P1 region means that the optimization of a conformation in this region leads to the complex-P1. In the product region, a periodic motion of the proton (H_{3a} atom) is observed between O_3 and Cl (Fig. 3f). A snapshot of this region is shown in Fig. 5f. Thermal motion of the system allows an internal rotation about the C–O single bond, which lets the proton H_{lb} interact more favorably with the chloride ion, as indicated in the structure at 314 fs (Fig. 5e). Optimization of the conformation of the trajectory in this phase leads to another product complex (complex-P2). Along the trajectory up to 500 fs, most of the conformations are within the complex-P1 region, although a few conformations are within the complex-P2 region.

The whole trajectory of the system was followed until 2000 fs. The potential energy of the system becomes lower at around 880 fs, which corresponds to the time when the distance between Cl and H_{lb} becomes shorter, implying that the system is now in the complex-P2 region. Then around 980 fs,

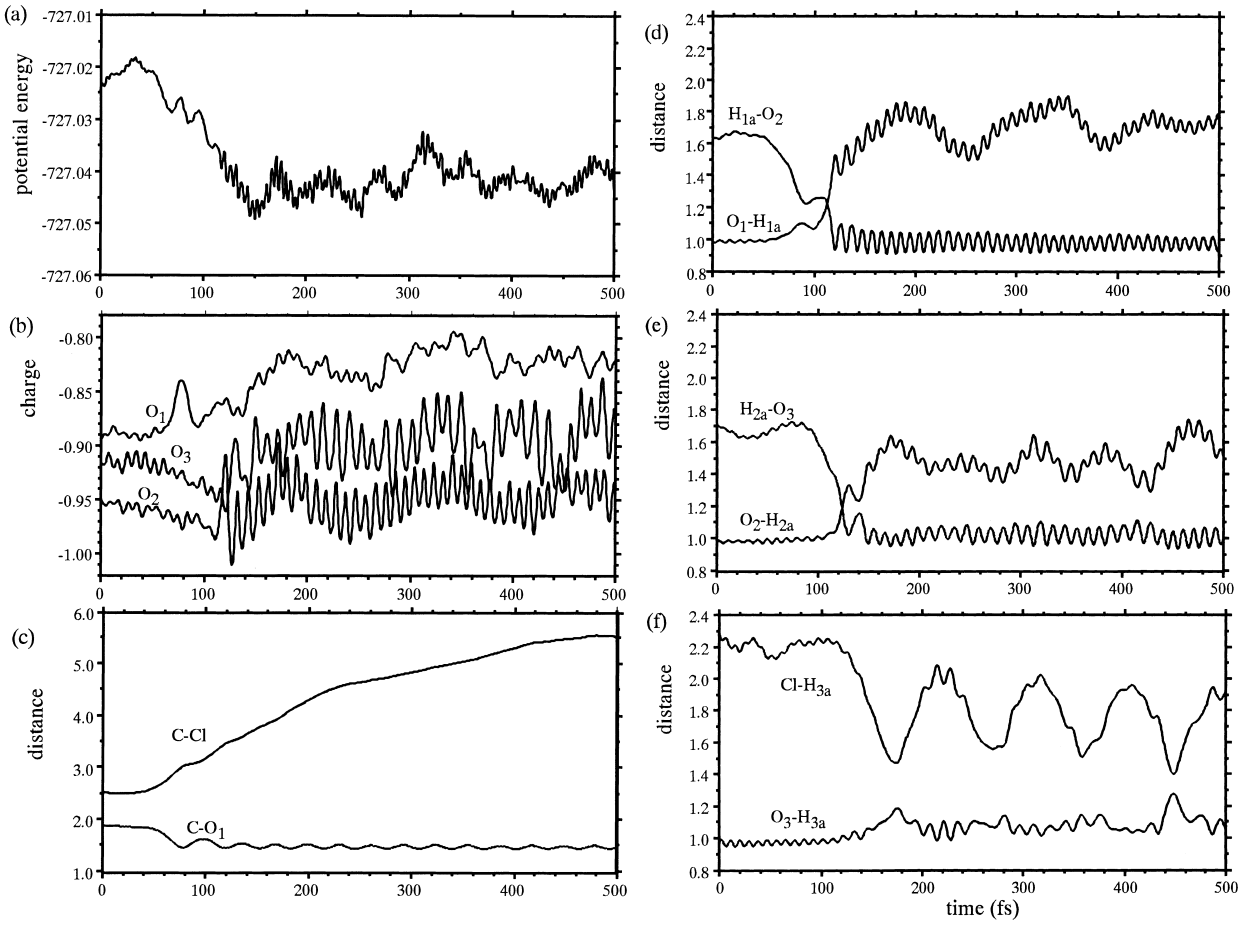

Fig. 4. Trajectory of a forward reaction (case-1) for MeCl hydrolysis from the TS toward complex-P1: (a) potential energy (in hartree); (b) the atomic charges; (c) the atomic distances (in Å) between C and Cl and between C and O_l; (d) between O_l and H_{la} and between H_{la} and O_2; (e) between O_2 and H_{2a} and between H_{2a} and O_3; (f) between Cl and H_{3a} and between O3 and H_{3a}.

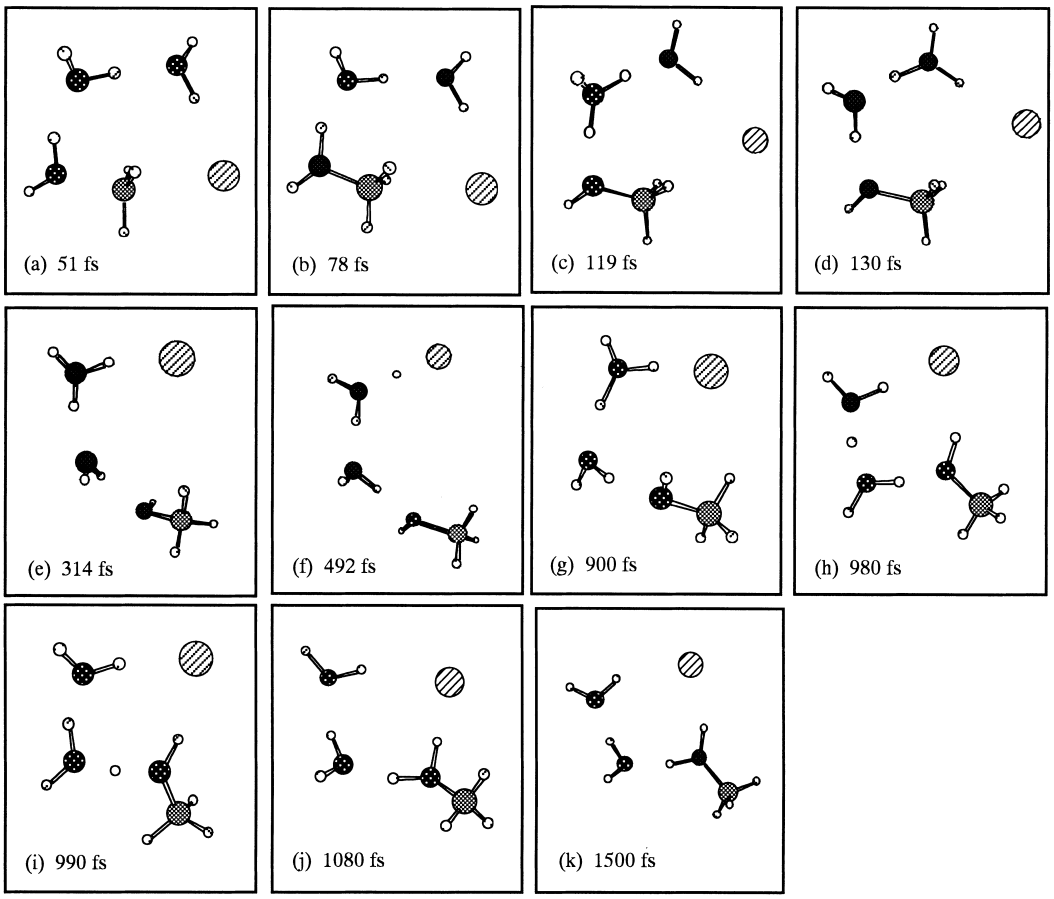

Fig. 5. Snapshot structures along the forward trajectory (case-1) at: (a) 51 fs; (b) 78 fs; (c) 119 fs; (d) 130 fs; (e) 314 fs; (f) 492 fs; (g) 900 fs; (h) 980 fs; (i) 990 fs; (j) 1080 fs; (k) 1500 fs.

another noticeable change is observed; reversed, nearly concerted proton transfers bring the system to the complex-F region. The proton H_{2a}, which had transferred to O_3 at around 130 fs, goes back to O_2 at around 980 fs; the proton H_{1a}, which had transferred to O_2 at around 120 fs, goes back to O_1 at around 990 fs. Optimization of a conformation in the region after the back proton transfers leads to complex-F (Fig. 3f). The final product (complex-F, Fig. 3f) looks as if it were a direct adduct of H_2O to the CH_3^+ moiety, but in fact successive proton-transfer steps are involved in this process.

Forward Reaction, 2. There is a different type of trajectory (case-2) toward the product state; the structures of some points along such trajectory are shown in Fig. 6a–f. Optimization procedures on some points along the trajectory confirmed that the system is in the complex-P1 region before 120 fs and in the complex-P2 region after 120 fs. It was found that the proton transfers occurs only in the complex-P2 region. The system moves to the complex-P2 region without going through a series of proton transfers in the complex-P1 region. This is because the H_{1b} atom faces the Cl atom at a rather early stage in the transition state region; the phenomenon is brought about by thermal motions generated by random initial velocities. Continuation of this simulation until 2000 fs showed that the system stays in the complex-P2 region until around 950 fs, when the nearly concerted back proton transfers begin to occur and bring the system to the complex-F region, in a similar manner to that found in the simulation described above.

In short, the ab initio MD simulations exhibit dynamic features of the S_N2 reaction of methyl chloride with three water molecules, which can be regarded as a prototype of the methyl chloride hydrolysis in aqueous solution. The backward reaction and the forward reaction show some different features. The backward reaction proceeds very quickly; the attacking water molecule goes away from the methyl chloride soon after the TS. In the forward reaction, the attacking water molecule keeps two hydrogen atoms in the transition region; this period lasts around 100 fs. Then nearly concerted proton transfers occur and an intermediate complex (complex-P1 region) is formed around 150 fs. With further thermal motions, the system reaches the final complex region after 1000 fs. The trajectories from the complex-R region through TS to the complex-P1 region are those which trace the IRC path. Other trajectories, which are different from the IRC path, were also observed for the forward reaction, in which the system moves to another intermediate complex (complex-P2) region, and after the nearly concerted proton transfers the product is formed. The IRC path is not the only path along which the reaction proceeds at finite temperature. In either pathway, the nearly concerted back proton transfers lead the system to the same final product. The present study typically showed that the ab initio MD simulation is a powerful technique to explore the reaction processes at finite temperature.

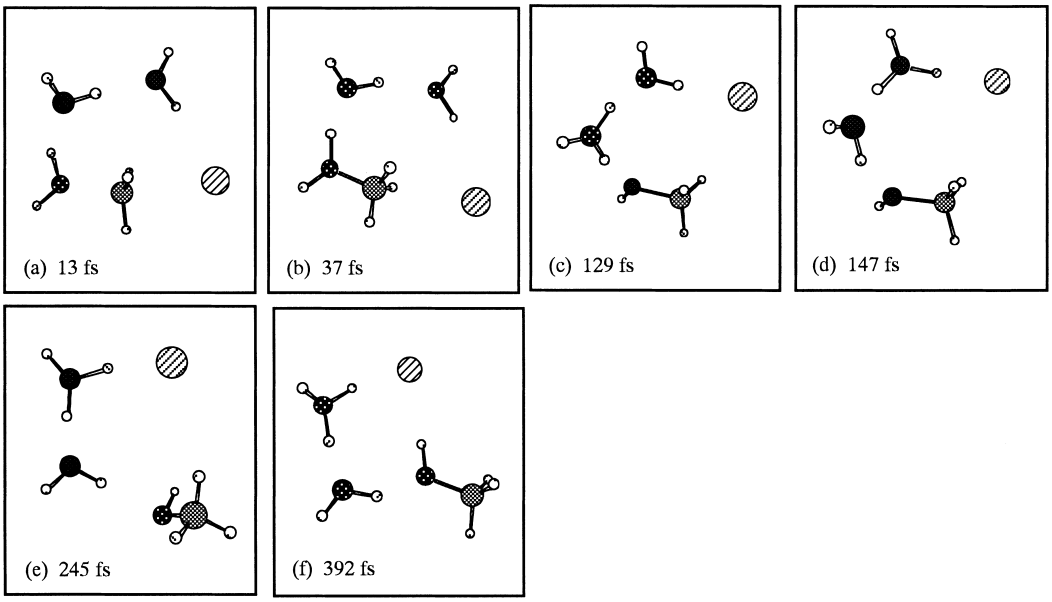

Fig. 6. Snapshot structures along the trajectory of a forward reaction (case-2) at: (a) 13 fs; (b) 37 fs; (c) 129 fs; (d) 147 fs; (e) 245 fs; (f) 392 fs.

S_N1 Reaction

The hydrolysis of *t*-BuCl is a multi-step reaction with the intervention of a series of ion-pair intermediates (Scheme 1).[52] This Winstein ion-pair scheme was proposed on the basis of kinetic behavior in aq alcoholic solvents. The mechanism considers three ionic intermediates: a contact ion pair (CIP), a solvent-separated ion pair (SSIP), and free ions. It should be noted, however, that in pure water solvent a water molecule traps *t*-Bu cation in ion pair stages (CIP and SSIP) before it goes to free ions. Product stereochemistry in aq alcohol showed net inversion of configuration,[53] consistent with the trap by the solvents at the CIP and/or SSIP stages. Any computational method aimed at describing the role of solvent molecules during the reaction at the molecular level must reproduce events that occur in a real reaction. In the case of hydrolysis of *t*-BuCl, these are the reactions of the ion-pair intermediate to give substitution by a water molecule with the inversion of configuration as a major product, together with substitution with the retention of configuration, and the ion-pair return to regenerate *t*-BuCl. Elimination is an important reaction channel in less polar solvents,[54] but it has little relevance in pure water.

Since the description of *t*-BuCl hydrolysis is most challenging, a number of computational methods have been applied to this reaction. Jorgensen et al., in a pioneer work in this field, carried out Monte Carlo computation on the hydrolysis and demonstrated that CIP exists with the C–Cl atomic distance of 2.9 Å but that SSIP and free ions are not energetically distinct species.[55] QM/MM computations by Hartsough and Merz revealed that CIP exists with the C–Cl distance of 2.9 Å, that the barrier to the backward reaction to *t*-BuCl from CIP is 8.8 kcal/mol and that the overall barrier of the reaction is 19.5 kcal/mol, which exists between CIP and SSIP.[56] These studies do not include nucleophilic solvent molecules that play an essential role in the reactions of ion pairs to give the products. We have carried out ab initio direct-MD as well as QM/MM-MD simulations of CIP, and showed that the simulation can reproduce all possible reaction channels of CIP in water.[57] All calculations were carried out with HONDO[51] using HF/3-21G for the QM part and TIP3P with vibrational potentials for internal vibrations of water for the MM water molecules.[58]

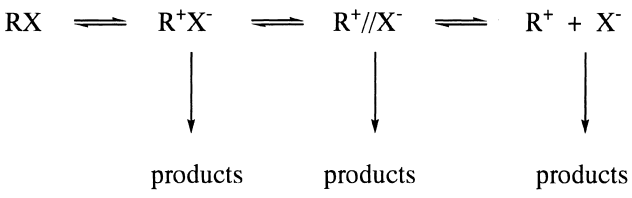

Scheme 1. Winstein ion-pair scheme.

Ab Initio MD Simulations from the Contact Ion Pair. In order to perform MD simulations for the reactions of CIP in water, a local minimum structure of CIP should have been determined in advance. A CIP complex cannot be localized as an intermediate in the gas phase, since it is not a stable local minimum without solvent molecules. We could obtain the CIP intermediate of the hydrolysis of *t*-BuCl, in which H_2O, *t*-Bu^+, and Cl^- are linearly aligned, by considering 10 bridging water molecules explicitly. As in the case of MeCl hydrolysis, several water molecules form a hydrogen-bond network between the H_2O and the leaving Cl atom (Fig. 7). By means of the frequency analysis, this structure was confirmed as a local minimum.

Ab initio MD simulations starting from the CIP gave two types of trajectories, one going back to the reactant state and the other giving the substitution product of the inversion of configuration. Figure 8 shows a series of the snapshots along a trajectory that leads to the product state. Around 400 fs, a proton transfer from the attacking water molecule toward a water molecule next to the attacking water occurs, and then several

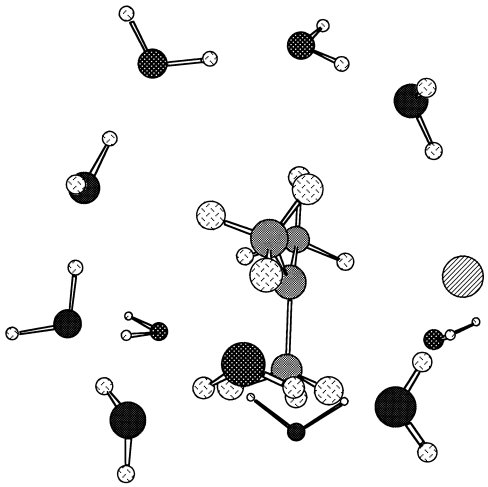

Fig. 7. Optimized CIP structure of *t*-BuCl with 10 water molecules (HF/3-21G).

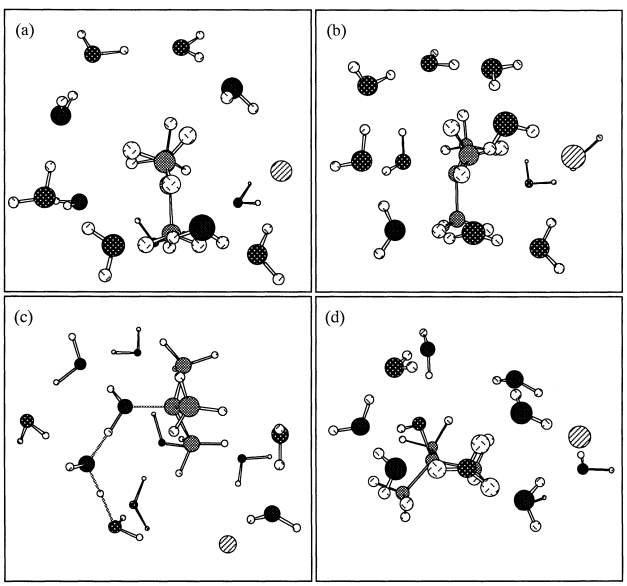

Fig. 8. A series of the snapshots along a trajectory toward the product state starting from the CIP complex. (a) at 100 fs; (b) at 300 fs; (c) at 400 fs, (d) at 500 fs.

consecutive proton transfers takes place. The product state was comprised of HO–C$(CH_3)_3$, H_3O^+, $9H_2O$, and Cl^-. Clearly the system of *t*-BuCl with 11 water molecules can be used as a model system to mimic the S_N1 reaction at least in part.

QM/MM-MD Simulations from the Contact Ion Pair. The QM/MM method is considered to be a suitable method to obtain a more realistic picture of *t*-BuCl hydrolysis. We used the intermediate CIP structure of all QM (HF/3-21G) as a starting geometry; we kept 4 water molecules on the rear side of *t*-BuCl and 3 water molecules around Cl as QM, and put additional 79 MM water molecules around. This CIP complex is shown in Fig. 9. Fourteen QM/MM-MD simulations starting from this CIP complex were performed. Five of the 14 trajectories went back toward the reactant state directly from CIP; six of them led to the substitution product with the inversion of

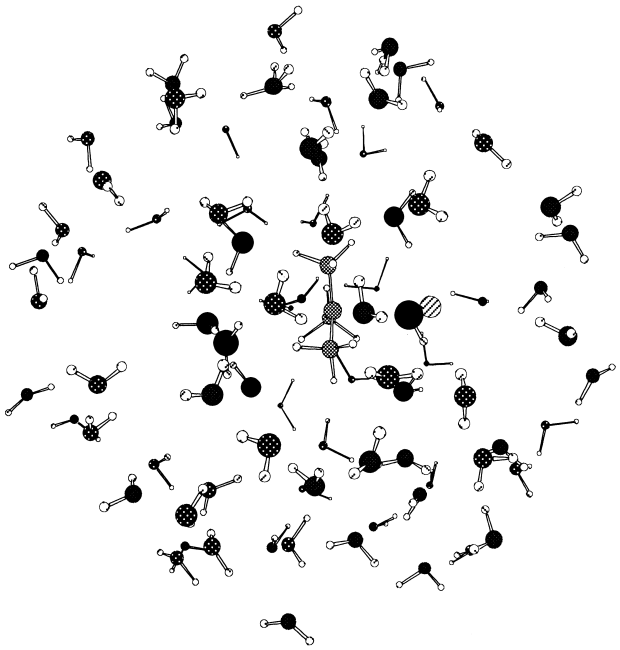

Fig. 9. The CIP structure with 7 QM (HF/3-21G) water molecules and 79 MM (TIP3P) water molecules. The O atoms of the QM part are shown with filled symbols.

configuration; three of them gave the substitution product with the retention of configuration. Figure 10 shows two snapshots along a trajectory which went toward the inversion product, and Fig. 11 shows two snapshots along a trajectory which went toward the retention product. In the latter case, one of the water molecules that are originally hydrogen-bonded to Cl^- attacks *t*-Bu^+. As far as we know, this is the first report to show computationally that the retention product can be obtained in the S_N1 reaction from the CIP intermediate. Calculations using a larger basis set with a larger number of MM water molecules would allow us to fully analyze the product forming processes in *t*-BuCl hydrolysis.

S_N2/ET Borderline Reaction

Organic reactions that proceed via a region mechanistically intermediate between two extremes are called borderline reactions.[45,59] The analysis of the borderline nature of the reactions is not straightforward. One explanation suggests that borderline reactions proceed via two distinct routes and the observed experimental data reflects a chemical dynamics average of the two distinct processes. A second explanation assumes that these reactions proceed via a single TS of intermediate character. Examples of borderline reactions are found in combined electron-transfer (ET)/substitution (S_N2) reactions, depending on the donor and/or acceptor molecules.[60–63]

The reaction of CH_3Cl with a $H_2C{=}O$ radical anion (Eq. 2) belongs to this class of reactions. Sastry and Shaik[64] carried out ab initio MO calculations for this reaction and reported the

$$H_2C{=}O^{\bullet -} + CH_3{-}Cl \rightarrow \underset{\text{(ET product)}}{H_2C{=}O + CH_3^{\bullet}} + Cl^- \quad \text{and/or}$$

$$\underset{(S_N2\ \text{product})}{CH_3CH_2O^{\bullet}} + Cl^- \qquad (2)$$

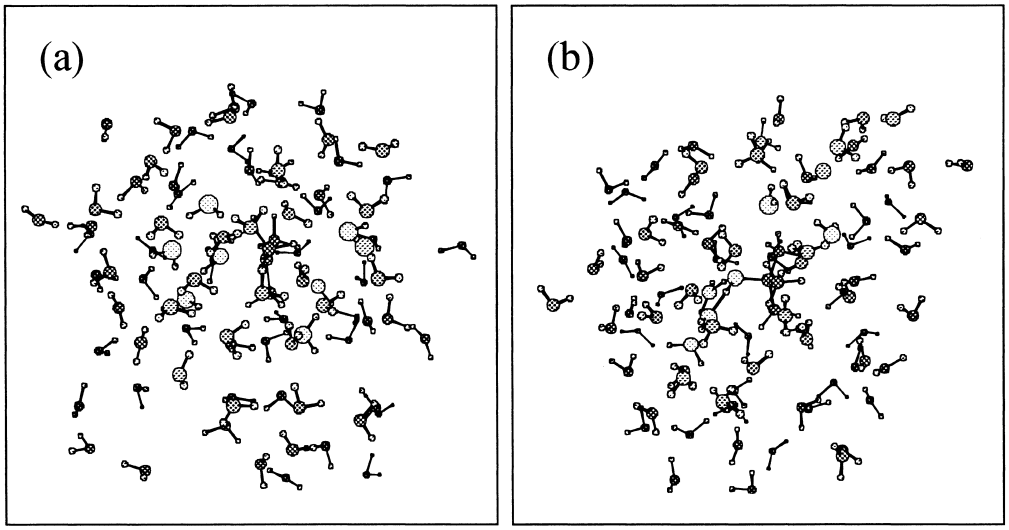

Fig. 10. A series of the snapshots during a trajectory toward the inversion substitution starting from the CIP complex. (a) at 500 fs; (b) at 1000 fs.

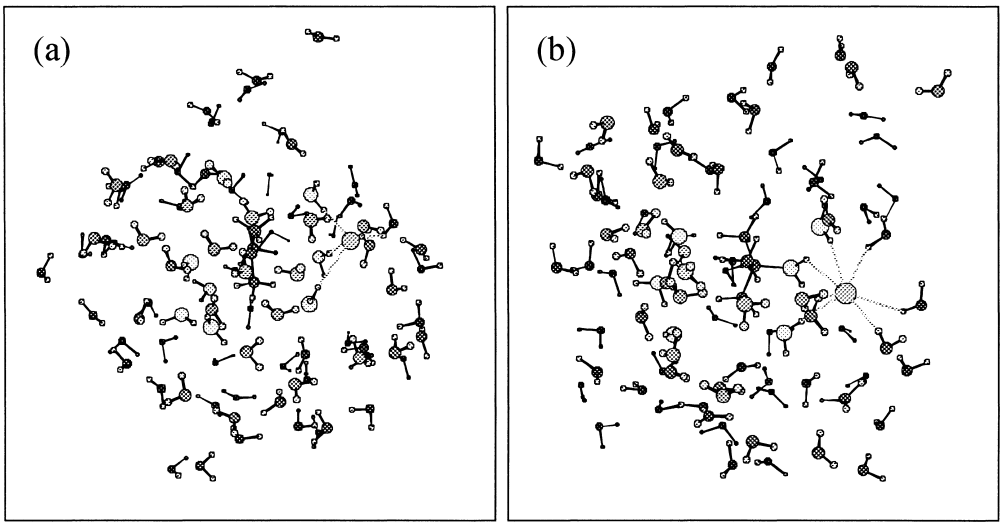

Fig. 11. A series of the snapshots during a trajectory toward the retention substitution starting from the CIP complex. (a) at 300 fs; (b) at 500 fs.

existence of a TS leading to an ET product. Bertran et al. suggested that the same TS could be viewed as an S_N2 TS involving the carbon atom of $H_2C{=}O$ radical anion as a nucleophilic center.[65] The origin of the different mechanistic assignment for the TS was analyzed by Sastry and Shaik on the basis of the potential energy surface calculated at the UHF/6-31G* level of theory.[66] These authors showed that the reaction path descends from a broad saddle point to a flat ridge that separates the ET and S_N2 products. After entering the flat ridge region the path bifurcates to the two product states. Different reaction-path following methods gave different mechanistic assignments:[66] the steepest descent path in *Z*-matrix internal coordinates leads directly to the ET product whereas the path in mass-weighted internal coordinates leads to a ridge and descends to the S_N2 product. However, these discussions based on the MO calculations are only relevant for the reaction at 0 K.[66] The interpretation of the reaction mechanism ought to rely on reaction dynamics at finite temperature instead. Ab initio direct-MD calculations where the energy and the forces of the system are computed from an ab initio MO treatment are a means to obtain the desired dynamical characterization.

Ab initio MD simulations were carried[27] out for the reaction of CH_3Cl and a $H_2C{=}O$ radical anion using the program packages of HONDO.[51] The initial atomic velocities were assigned from a random distribution with the total kinetic energy being consistent with the simulation temperatures (100 K, 298 K, and 400 K). A velocity re-scaling algorithm similar to the constant-temperature algorithm of Berendsen et al.[44] was used to mimic the solvent effects, and two different values of a solute-solvent relaxation time τ (50 fs and 2000 fs) were adopted in the calculations. Constant-energy simulations were also performed (i.e., $\tau = \infty$) using the same initial velocities as were

used in the "velocity re-scaling" simulations. Fifty-one MD simulations were performed for each relaxation time with the UHF/6-31+G* level of theory.

Dynamics for the Borderline Reaction. The energy profile, the stationary point structures, and the potential energy surface of $CH_2O^{\bullet-}$ with CH_3Cl are depicted in Fig. 12. The ridge separating the reactant valley from the product valley and the ridge separating the ET valley from the S_N2 valley are seen in the 3D potential energy surface (Fig. 13). In the MD simulations starting from the S_N2-like TS, four types of trajectories

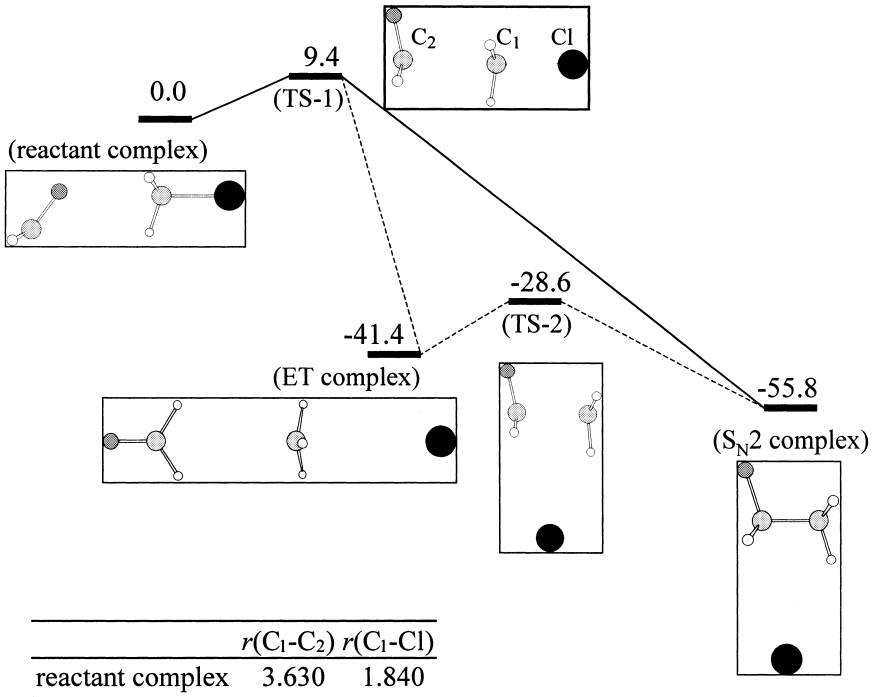

	$r(C_1\text{-}C_2)$	$r(C_1\text{-}Cl)$
reactant complex	3.630	1.840
TS-1	2.563	2.100
S_N2 complex	1.525	3.790
TS-2	2.085	3.734
ET complex	3.721	3.826

Fig. 12. The UHF/6-31+G* energy profile of the reaction of $CH_2O^{\bullet-}$ with CH_3Cl. Relative energies are in kcal/mol. The C_1–C_2 and C_1–Cl atomic distances at stationary points are shown in Å.

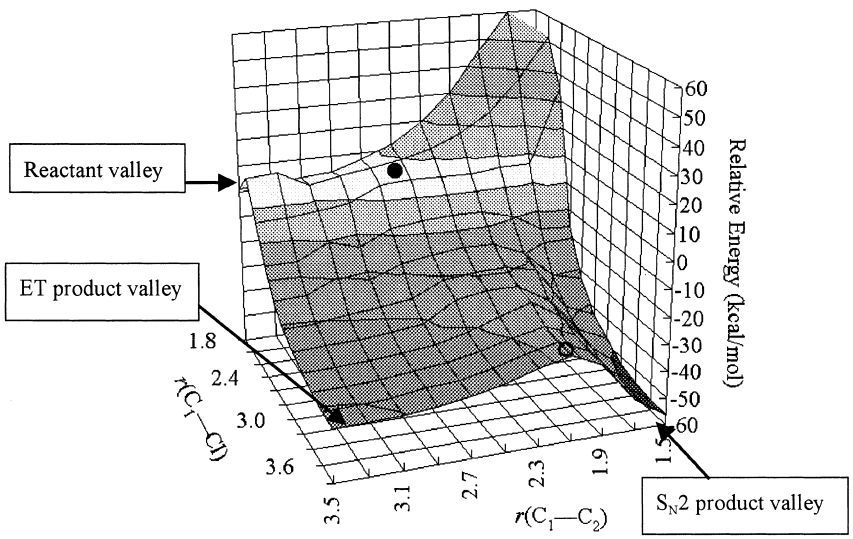

Fig. 13. Three-dimensional potential energy surface at UHF/6-31+G*. Distances are in Å. The contours are spaced by 10.0 kcal/mol. The filled circle indicates the position of TS-1, and the open circle TS-2.

were observed: those leading back to the reactants, those leading to the S_N2 product, those passing through the S_N2 valley and crossing over to the ET valley, and finally those going to the ET valley directly. The number of the trajectories of each type is summarized in Table 1 for each of the three relaxation times used in the simulations. Thus, the present dynamics calculations clearly confirm that the TS can lead directly to either the ET or the S_N2 product even though the TS has a nearly collinear C_2–C_1–Cl arrangement as well as partial C_2–C_1 and C_1–Cl bonds, in accord with the characteristics of S_N2 TS's.

Representative trajectories (3 for each type) are plotted in Fig. 14, and the variations in the atomic spin density on atom C_1 for these trajectories are shown in Fig. 15. The essential features of the reactions are completed when the molecular system reaches a region ($r(C_1–C_2) < 1.7$ Å, $r(C_1–Cl) > 3.0$ Å) for the S_N2 reaction, and a region ($r(C_1–C_2) > 2.3$ Å, $r(C_1–Cl) > 3.4$ Å) for the ET reaction. Line a in Fig. 15 is the trajectory that goes directly towards the ET valley. In ~30 fs starting from the TS, the spin localization on atom C_1 is almost complete and the system proceeds directly towards the ET valley. In the trajectory going towards the S_N2 valley (Fig. 15, line c), the spin localization at C_1 occurs concomitant with the elongation of the C–Cl bond after ~20–30 fs starting from the TS. At ~40–50 fs, the spin re-localization begins in the CH_2O–CH_3 fragment, and finally the spin localizes on the O atom. Line b in Fig. 15 shows the variation in the spin density on atom C_1 in the trajectory going towards the S_N2 valley first and then crossing over the ridge towards the ET valley. The variations in the C_1 spin density (Fig. 15, line b) together with the atomic distance variations (Fig. 14) clearly show that the S_N2 reaction is completed in ~60–80 fs, and then the second step of the crossing over the ridge begins at ~100 fs.

Table 1. The Number of Trajectories towards Each of the Stationary States

τ[a)]	Reactant	S_N2	S_N2 then ET	ET directly
50	12	36	0	3
2000	12	32	4	3
∞	12	31	5	3

a) The relaxation time used in the simulations.

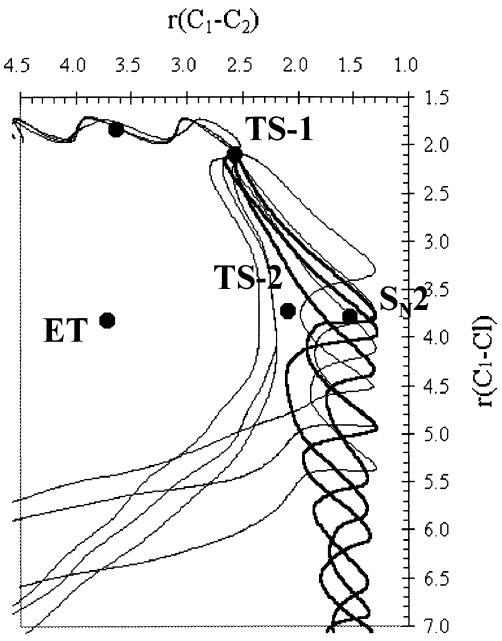

Fig. 14. MD trajectories starting from TS-1 of the reaction of $CH_2O^{\bullet-}$ with CH_3Cl with the solute-solvent relaxation time of 2000 fs at 298 K. Distances are in Å.

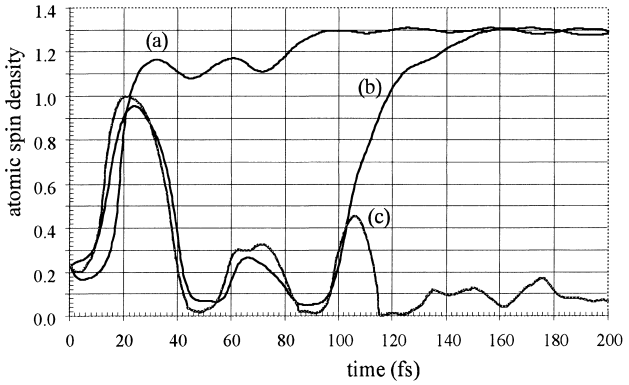

Fig. 15. The variation in the atomic spin density on C_1 atom: (a) In the trajectories directly towards the ET product valley; (b) In the trajectories first towards the S_N2 product valley and then towards the ET valley; (c) In the trajectories towards the S_N2 product valley only.

It is noticeable that starting from the TS, the system reaches the valley in ~70–80 fs in any of the trajectories observed here. The fate of the reaction, i.e., whether it proceeds towards the reactant region (12 trajectories), the S_N2 region (36 trajectories), or the ET region directly (3 trajectories) in this initial step, is essentially sealed early and the solute–solvent relaxation does not really affect it.

The IRC path and selected MD trajectories (τ = 2000 fs) obtained at temperatures of 100, 200, and 400 K with identical initial velocity directions but with varied velocity amplitudes are shown in Fig. 16. They are superimposed over the 2D map of the potential energy surface. These trajectories follow the IRC path at the lower temperature (100 K), whereas at higher temperatures the kinetic energy affects the reaction. One of the trajectories goes towards the reactant complex at 100 K but it evolves directly into the ET product at 200 K. Two other trajectories that lead to the S_N2 product at the lower temperatures evolve directly towards the ET product at the higher temperatures (298 K and 400 K).

Shaik et al. carried out direct MD simulations on the same system using similar levels of theory but with different initial energy distributions.[28] Comparison of the two different sets of simulations, those in Refs. 27 and 28, further confirmed that the kinetic energy of reacting species plays an important role in controlling the pathway of organic reactions.

Characteristics of Trajectories of the ET and S_N2 Routes. The remaining question is what the individual S_N2 and ET trajectories look like. Figure 17 shows the results of one of the simulations that gave the ET product. The changes in the potential energy (Fig. 17a) and in the atomic distances between C_1–Cl, C_1–C_2, and C_2–O (Fig. 17b) for 300 fs reveal that the trajectory can be divided into three phases; in phase I

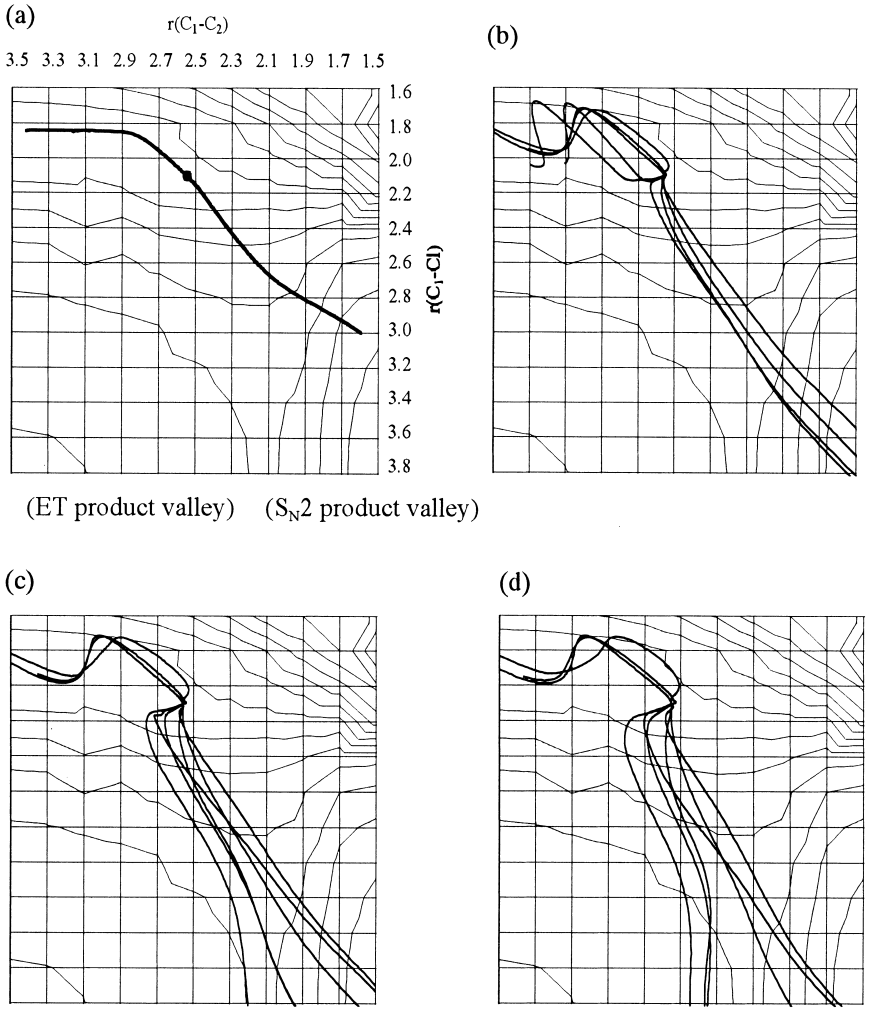

Fig. 16. (a) IRC path on the potential energy map. The dot indicates TS-1. (b) MD trajectories at 100 K. (c) MD trajectories at 200 K. (d) MD trajectories at 400 K. Distances are in Å and relative energy contours are spaced by 10.0 kcal/mol.

(∼30 fs) the potential energy and atomic distances do not change much; in phase II (∼200 fs) the energy starts to decrease and then stays constant, and the C_1–Cl atomic distance increases monotonically whereas the C_1–C_2 distance decreases and stays at 2.1 Å until 200 fs; in phase III (200 fs–) the potential energy becomes lower again, the C_1–Cl distance now becomes constant, and the C_1–C_2 distance increases up to 4.5 Å. The variations in the Mulliken group charges (Fig. 17c) and spin density (Fig. 17d) exhibit a sudden change in a later part of phase I. The group charge on the H_2C=O moiety decreases from −0.75 at 15 fs to −0.04 at 30 fs, and the total spin density on H_2C=O decreases from 0.78 to 0.02 in the same period of time. Apparently, rapid electron reorganization takes place here on the way to the ET product state. The methyl group ends up with an unpaired electron and there is essentially no spin density on Cl. After this electron reorganization, the group charge on H_2C=O stays nearly constant at −0.1 and that on CH_3 at +0.1 in phase II. The spin density on Cl stays nearly constant at 0.0 whereas that on CH_3 varies from 0.80 to 1.00. The variations of the spin density on the H_2C=O substructure are noticeable; the total spin density nearly equals zero, yet the alpha and the beta spins tend to be separated, one on CH_2 and the other on O, akin to a diradical character within the molecule. In phase III the two carbon centers begin to move away from each other, giving the methyl radical and formaldehyde.

Figure 18 depicts one of the simulations that give the S_N2 product. The trajectory here is much simpler than the ET trajectories. The changes in the potential energy (Fig. 18a) and in the atomic distances between C_1–Cl, C_1–C_2, and C_2–O (Fig. 18b) for 300 fs indicate that the C_1–C_2 bond formation and the C_1–Cl bond breaking occur in a concerted manner soon after the trajectory leaves the TS. The substitution is essentially completed by 50 fs and only the translational separation of the CH_3CH_2O radical and the Cl anion takes place thereafter. The changes in the Mulliken atomic charges and spin density were found to be consistent with the S_N2 process; Cl is formed as the anion and O becomes a radical center. Some simulations were performed by using the CASSCF(4o,5e) level of theory, which gave essentially the same results as the HF calculations.

In conclusion, the direct-MD simulations suggest that, in the reaction of $CH_2O^{\bullet -}$ and CH_3Cl as a prototype of borderline reactions, the S_N2-like TS yields intrinsically the S_N2 product. At finite temperature, however, a route opens up in which the

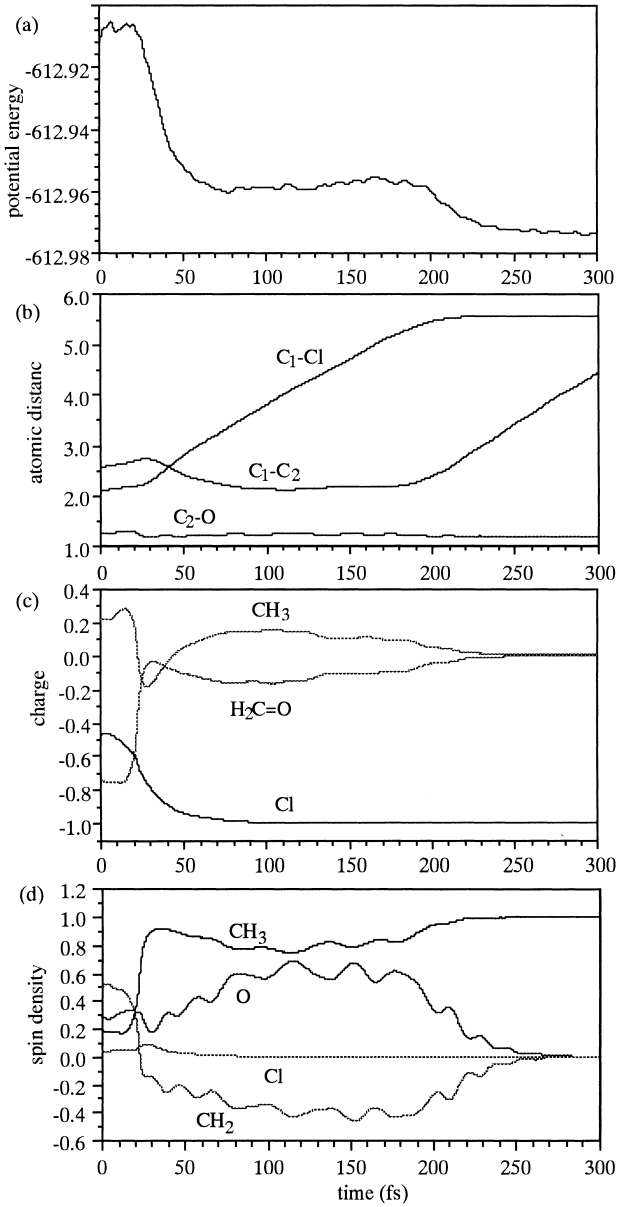

Fig. 17. Trajectory to the ET product. Variation in (a) potential energy, (b) atomic distances, (c) the Mulliken group charge, and (d) spin density.

system may evolve either directly or indirectly towards the ET product after passing over the S_N2-like TS. Such results imply that the TS characteristics themselves do not always dictate the reaction mechanism and that the formation of two different products does not necessarily mean the presence of two independent pathways with different TS's. A possible occurrence of branching from single TS to several products introduces additional complexities in mechanistic assignment for borderline reactions.[67] Furthermore, an observation that more ET product is formed at a higher temperature would often be taken as an indication that the reaction would follow two competitive routes with, as in the present case, a higher activation energy for the ET route than for the S_N2 route. The present analysis offers an alternative interpretation that a similar temperature

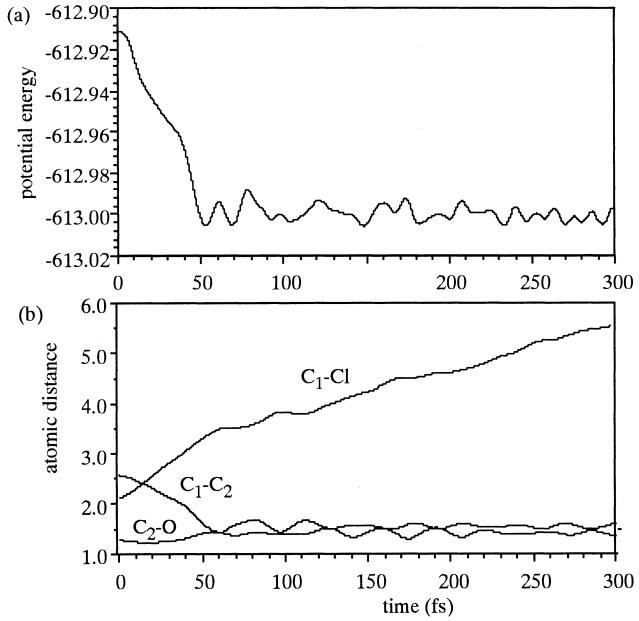

Fig. 18. Trajectory to the S_N2 product. Variation in (a) potential energy in hartree and (b) atomic distances.

effect on the product distribution can also arise from traversing single TS and undergoing temperature-mediated mechanisms to different products for a borderline reaction. Characteristic features of each process are also demonstrated clearly by the analyses of the trajectories. Such dynamic characteristics can only be treated with accuracy by the ab initio direct-MD simulations.

Epilogue

The theory of organic reactions has been developed mostly based on physical organic experiments, in which observable quantities are the average of the behaviors of a large number of reacting particles. Experimental results give inherently only an averaged picture of chemical reactions. In contrast, computational methods described above can give information of each reacting species at the molecular level. According to traditional interpretation of chemical reactivity, the reaction rate and hence the product selectivity are governed by the energy of the TS and its variation. However, as described in this account, this was found not universally true. Ab initio direct-MD simulations revealed that in a certain reaction of mechanistic borderline, a common TS could give two types of products and that the product ratio might not be governed by the relative energy of two independent TSs, but by the kinetic energy and the nature of the dynamics. A similar phenomenon of "dynamics-driven reaction path" has also been observed for an intramolecular rearrangement reaction.[68] Here it was shown that the reaction pathway did not follow the minimum energy path determined by MO calculations, but was rather controlled by the dynamics of the reaction. These results imply that the organic reactivity theory must consider the effect of dynamics explicitly. It should also be noted that the combined QM/MM method is becoming a practical tool to analyze organic reactions in solution. We expect that computational methods outlined in this

article should serve as a means to facilitate development of a new reaction theory in the next decade.

The authors acknowledge the invaluable contributions of Dr. Michel Dupuis, Pacific Northwest National Laboratory, USA. The studies described here were partly carried out at the Research Center for Computational Science, Okazaki National Research Institute.

References

1 M. P. Allen and D. J. Tildesley, "Computer simulations of liquids," Oxford University Press, Oxford (1987).

2 D. G. Truhlar, "The reaction path in chemistry: Current approaches and perspectives," ed by D. Heidrich, Kluwer, Dordrecht, The Netherlands (1995), p. 229.

3 R. Car and M. Parrinello, *Phys. Rev. Lett.*, **55**, 2471 (1985).

4 J. C. Greer, R. Ahlrichs, and I. V. Hertel, *Z. Phys. D*, **18**, 413 (1991).

5 B. Hartke and E. A. Carter, *Chem. Phys. Lett.*, **189**, 358 (1992).

6 S. A. Maluendes and M. Dupuis, *Int. J. Quantum Chem.*, **42**, 1327 (1992).

7 E. Uggerud and T. Helgaker, *J. Am. Chem. Soc.*, **114**, 4265 (1992).

8 J. Jellinek, V. Bonacic-Koutecky, P. Fantucci, and M. Wiechert, *J. Chem. Phys.*, **101**, 10092 (1994).

9 D. Reichardt, V. Bonacic-Koutecky, P. Fantucci, and J. Jellinek, *Chem. Phys. Lett.*, **279**, 129 (1997).

10 I. Tunon, M. T. C. Martins-Costa, C. Millot, and M. F. Ruiz-Lopez, *J. Chem. Phys.*, **106**, 3633 (1997).

11 R. Steckler, G. M. Thurman, J. D. Watts, and R. J. Bartlett, *J. Chem. Phys.*, **106**, 3926 (1997).

12 D. Wei and D. R. Salahub, *J. Chem. Phys.*, **106**, 6086 (1997).

13 H. Yamataka, M. Aida, and M. Dupuis, *Chem. Phys. Lett.*, **292**, 474 (1998). M. Aida, H. Yamataka, and M. Dupuis, *Theor. Chem. Acc*, **102**, 262 (1999).

14 G. Li and W. L. Hase, *J. Am. Chem. Soc.*, **121**, 7124 (1999).

15 a) G. H. Peslherbe, H. Wang, and W. L. Hase, *J. Am. Chem. Soc.*, **118**, 2257 (1996). b) G. H. Peslherbe, H. Wang, and W. L. Hase, *J. Chem. Phys.*, **102**, 5626 (1995), and references cited herein.

16 a) H. Tachikawa, *J. Phys. Chem. A*, **104**, 497 (2000). b) H. Tachikawa and M. Igarashi, *Chem. Phys. Lett.*, **303**, 81 (1999).

17 H.-H. Bueker, T. Helgaker, K. Ruud, and E. Uggerud., *J. Phys. Chem.*, **100**, 15388 (1996).

18 Y. Ishikawa and R. C. Binning, Jr., *Chem. Phys. Lett.*, **343**, 353 (2001). Y. Ishikawa and R. C. Binning, Jr., *Chem. Phys. Lett.*, **343**, 597 (2001).

19 T. Helgaker, E. Uggerud, and H. A. Aa. Jensen, *Chem. Phys. Lett.*, **173**, 145 (1990). E. L. Øiestad and E. Uggerud, *Int. J. Mass Spectrom. Ion Processes*, **165/166**, 39 (1997).

20 H. Wang, E. M. Goldfield, and W. H. Hase, *J. Chem. Soc., Faraday Trans.*, **93**, 737 (1997).

21 T. Takayanagi, Y. Kurosaki, and H. Tachikawa, *Int. J. Mass Spectrom.*, **176**, 227 (1998).

22 X. Li, J. M. Millan, and H. B. Schlegel, *J. Chem. Phys.*, **113**, 10062 (2000). W. Chen, W. L. Hase, and H. B. Schlegel, *Chem. Phys. Lett.*, **228**, 436 (1994).

23 H. Takahashi, T. Hori, T. Wakabayashi, and T. Nitta, *J. Phys. Chem. A*, **105**, 4351 (2001).

24 K. M. Forsythe, S. K. Gray, S. J. Klippenstein, and G. E. Hall, *J. Chem. Phys.*, **115**, 2134 (2001).

25 Y. Kumeda, Y. Minami, K. Takano, T. Taketsugu, and T. Hirano, *J. Mol. Struct. (THEOCHEM.)*, **458**, 285 (1999).

26 R. L. Hayes, E. Fattal, N. Govind, and E. A. Carter, *J. Am. Chem. Soc.*, **123**, 641 (2001).

27 H. Yamataka, M. Aida, and M. Dupuis, *Chem. Phys. Lett.*, **300**, 583 (1999); H. Yamataka, M. Aida, and M. Dupuis, *Chem. Phys. Lett.*, **353**, 310 (2002).

28 V. Bakken, D. Danovich, S. Shaik, and H. B. Schlegel, *J. Am. Chem. Soc.*, **123**, 130 (2001).

29 T. Taketsugu, T. Yanai, K. Hirao, and M. S. Gordon, *J. Mol. Struct. (Theochem.)*, **451**, 163 (1998). T. Taketsugu and M. S. Gordon, *J. Phys. Chem.*, **99**, 8462 (1995).

30 D. Wei and D. R. Salahub, *J. Phys. Chem.*, **106**, 6086 (1997).

31 H. Tachikawa, *Phys. Chem. Chem. Phys.*, **2**, 839 (2000).

32 C. Doubleday, Jr., K. Bolton, and W. L. Hase, *J. Am. Chem. Soc.*, **119**, 5251 (1997); *J. Phys. Chem. A*, **102**, 3648 (1998); C. Doubleday, Jr., K. Bolton, G. H. Peslherbe, and W. L. Hase, *J. Am. Chem. Soc.*, **118**, 9922 (1996); K. Bolton, W. L. Hase, H. B. Schlegel, and K. Song, *Chem. Phys. Lett.*, **288**, 621 (1998); K. Bolton, H. B. Schlegel, W. L. Hase, and K. Song, *Phys. Chem. Chem. Phys.*, **1**, 999 (1999).

33 V. Moliner, A. J. Turner, and I. H. Williams, *J. Chem. Soc., Chem. Commun.*, **1997**, 1271; A. J. Turner, V. Moliner, and I. H. Williams, *Phys. Chem. Chem. Phys.*, **1**, 1323 (1999); J. A. Barnes and I. H. Williams, *J. Chem. Soc., Chem. Commun.*, **1996**, 193.

34 M. Garcia-Vioca À, Gonzáles-Lafont, and J. M. Lluch, *J. Am. Chem. Soc.*, **123**, 709 (2001); M. Garcia-Vioca, À. Gonzáles-Lafont, and J. M. Lluch, *J. Am. Chem. Soc.*, **121**, 9198 (1999).

35 K. Bolton, W. L. Hase, and C. Doubleday, Jr., *J. Phys. Chem. B.*, **103**, 3691 (1999)

36 A. González-Lafont, J. M. Lluch, and J. Bertrán, "Solvent Effects and Chemical Reactivity," ed by O. Tapia and J. Bertrán, Klumer Academic Publisher, Dordrecht (1996), pp. 125–177.

37 D. Marx, M. E. Tuckerman, J. Hutter, and M. Parrinello, *Nature*, **397**, 601 (1999); B. L. Trout, *Adv. Chem. Eng.*, **28**, 353 (2001).

38 N. Agmon, *Chem. Phys. Lett.*, **244**, 456 (1995).

39 Y. Xie, R. B. Remington, and H. F. Schaefer, *J. Chem. Phys.*, **101**, 4878 (1994).

40 L. Ojamae, I. Shavitt, and S. J. Singer, *Int. J. Quantum Chem.*, **29**, 657 (1995).

41 E. F. Valeev and H. F. Schaefer, *J. Chem. Phys.*, **108**, 7197 (1998).

42 D. J . Wales, *J. Chem. Phys.*, **110**, 10403 (1999).

43 M. Aida, Y. Yamane, T. Miyake, H. Yamataka, and M. Dupuis, unpublished.

44 H. J. C. Berendsen, J. P. M. Postma, W. F. van Gunsteren, A. DiNola, and J. R. Haak, *J. Chem. Phys.*, **81**, 3684 (1984).

45 C. K. Ingold, "Structure and Mechanism in Organic Chemistry," 2nd ed, Cornell University Press, London (1969).

46 H. Yamataka and M. Aida, *Chem. Phys. Lett.*, **289**, 105 (1998); M. Aida and H. Yamataka, *J. Mol. Struct. (THEOCHEM.)*, **461/462**, 417 (1999).

47 K. Fukui, *J. Phys. Chem.*, **74**, 4161 (1970).

48 K. Ishida, K. Morokuma, and A. Komornicki, *J. Chem.*

Phys., **66**, 2153 (1977).
49 M. H. Abraham and D. J. McLennan, *J. Chem. Soc., Perkin Trans. 2*, **1977**, 873.
50 S. G. Lias, J. E. Bartmess, J. L. Holmes, R. D. Levin, and G. W. Mallard, *J. Phys. Chem. Ref. Data, Suppl*., **17**, 1 (1988).
51 M. Dupuis, A. Marquez, and E. R. Davidson, "The program packages of HONDO," available from the Quantum Chemistry Program Exchange, Indiana University.
52 S. Winstein, E. Clippinger, A. H. Fainberg, and G. C. Robinson, *J. Am. Chem. Soc*., **76**, 2597 (1954).
53 A. Streitwieser, *Chem. Rev*, **56**, 571 (1956).
54 M. Cocirera and S. Winstein, *J. Am. Chem. Soc*., **85**, 1702 (1963).
55 W. L. Jorgensen, J. K. Buckner, S. E. Huston, and P. J. Rossky, *J. Am. Chem. Soc*., **109**, 1891 (1987)
56 D. S. Hartsough and K. M. Merz, Jr., *J. Phys. Chem*., **99**, 384 (1995).
57 M. Aida, H. Yamataka, and M. Dupuis, unpublished.
58 M. Aida, H. Yamataka, and M. Dupuis, *Int. J. Quantum Chem*., **77**, 199 (2000).
59 H. T. Lowry and K. S. Richardson, "Mechanism and Theory in Organic Chemistry," 3rd ed, Harper & Row, New York (1987).
60 H. Lunt, K. Daasberg, T. Lunt, and S. U. Pedersen, *Acc. Chem. Res*., **28**, 313 (1995). T. Lund and H. Lund, *Acta Chem. Scand., Ser. B*, **42**, 269 (1988).
61 J.-M. Savéant, *Adv. Phys. Org. Chem*., **26**, 1 (1990).
62 D. Lexa, J.-M. Savéant, K.-B. Su, and D.-L. Wang, *J. Am. Chem. Soc*., **110**, 7617 (1988).
63 N. Kimura and S. Takamuku, *J. Am. Chem. Soc*., **116**, 4087 (1994).
64 G. N. Sastry and S. Shaik, *J. Am. Chem. Soc*., **117**, 3290 (1995).
65 J. Bertran, I. Gallardo, G. Morene, and J.-M. Savéant, *J. Am. Chem. Soc*., **118**, 5737 (1996).
66 a) S. Shaik, D. Danovich, G. N. Sastry, P. Y. Ayala, and H. B. Schlegel, *J. Am. Chem. Soc*., **119**, 9237 (1997). b) G. N. Sastry and S. Shaik, *J. Am. Chem. Soc*., **120**, 2131 (1998). c) G. N. Sastry and S. Shaik, *J. Phys. Chem*., **100**, 12241 (1996).
67 B. K. Carpenter, *Acc. Chem. Res*., **25**, 520 (1992); M. B. Reys and B. K. Carpenters, *J. Am. Chem. Soc*., **120**, 1641 (1998), and references cited therein.
68 H. Yamataka, S. C. Ammal, M. Aida, and M. Dupuis, unpublished. Presented in part at the IXth Kyushu International Symposium on Physical Organic Chemistry, Fukuoka, Dec. 27–30 (2001).

Hiroshi Yamataka was born in Osaka in 1948. He received his Master's degree in 1972 from Osaka University. He jointed Professor Y. Yukawa's group as a Research Associate at the Institute of Scientific and Industrial Research, Osaka University before completing the doctoral course in 1974. He received his Doctoral degree in 1976 from Osaka University and spent postdoctoral years at the University of Arkansas (Professor A. Fry, 1976–1978). He was promoted to Assistant Professor in 1983 and to Associate Professor in 1988 at Osaka University. He moved to the Institute for Fundamental Research of Organic Chemistry, Kyushu University in 1994, and moved back to the Institute of Scientific and Industrial Research, Osaka University in 1996. His research interests include physical organic chemistry, in particular elucidation of organic reaction mechanisms by means of kinetic experiments and theoretical computations.

Misako Aida was born in Yokohama in 1955. She received her B.Sc. in 1977 and M.Sc. in 1979 from Ochanomizu University. She was appointed research associate at the National Cancer Center Research Institute in 1979. She received her Ph.D. in 1986 from Tokyo Institute of Technology and spent postdoctoral years at IBM in Kingston NY, USA (Dr. Enrico Clementi's group, 1988–1991). She started a research group at Hiroshima University as Professor in 1998. Her scientific interests are in the mechanism of molecular recognition and chemical reaction in solution and in biological systems.